


Article

The Effect of Cu Addition on Corrosion Resistance of Al-Si-Mg-Cr Alloy

Zhige Wang ¹, Liang Dong ¹, Bin Hu ² and Bin Chen ^{1,*} ¹ School of Materials Science and Engineering, Shanghai Jiao Tong University, Shanghai 200240, China² Shanghai Institute of Optics and Fine Mechanics, Chinese Academy of Sciences, Shanghai 201800, China

* Correspondence: steelboy@sjtu.edu.cn

Abstract: Two kinds of alloys with and without the addition of Cu, Al-7%Si-0.3%Mg-0.3%Cr and Al-7%Si-0.3%Mg-0.3%Cr-1.5%Cu, are studied in this work. The addition of Cu can notably improve notably the strength of Al alloy but it reduces its corrosion resistance. In this study, the electrochemical workstation is used to measure the open circuit potential and polarization curve of alloys and immersion corrosion is carried out. SEM and TEM images are taken before and after immersion corrosion to observe the pitting and intergranular corrosion of the alloy. Results show that the addition of Cu accelerates the immersion corrosion rate of Al alloy by 26.8% to 269.2%. This affects the peak ageing and overageing samples the most. The influence is less evident for underaged samples. At the same time, the addition of Cu aggravates the aggregation of pitting corrosion in the primary step of corrosion of Al alloy and the intergranular corrosion around and within the pitting hole. β'' -Mg₅Si₆ precipitates and θ'' -Al₃Cu precipitates are observed in Al-7%Si-0.3%Mg-0.3%Cr-1.5%Cu alloy. The Cu atoms occupy Si₃/Al site of β'' and segregate at the edge of β'' . It is believed that the deterioration of corrosion performance essentially is attributed to the Si-enriched particles, Al₁₃Cr₄Si₄ phase and the Cu-enriched precipitates, β'' -Mg₅Si₆ precipitates and θ'' -Al₃Cu precipitates.

Keywords: Al-Mg-Si cast alloy; precipitate; electrochemical; pitting



Citation: Wang, Z.; Dong, L.; Hu, B.; Chen, B. The Effect of Cu Addition on Corrosion Resistance of Al-Si-Mg-Cr Alloy. *Metals* **2023**, *13*, 795. <https://doi.org/10.3390/met13040795>

Academic Editor: Eric Hug

Received: 30 January 2023

Revised: 3 April 2023

Accepted: 12 April 2023

Published: 18 April 2023



Copyright: © 2023 by the authors. Licensee MDPI, Basel, Switzerland. This article is an open access article distributed under the terms and conditions of the Creative Commons Attribution (CC BY) license (<https://creativecommons.org/licenses/by/4.0/>).

1. Introduction

As an ideal alternative choice of steel to enlighten the weight, Al alloys are widely used in the automotive industry due to their excellent mechanical properties and resistance to corrosion. Different elements are added as alloy components to improve their performance. For example, Si and Mg are added to form a precipitation phase to strengthen Al alloy after heat treatment. Cr is added to counteract the negative effect induced by Fe and to refine the alloy grains by restraining them to grow [1,2]. As an important alloy element, Cu is also often added to enrich precipitation phases in Al alloys and thus augment the mechanical strength [3].

It believed that phases play a significant role in the corrosion of Al alloys. Previous studies show that the main corrosion for Al-Si-Mg alloy is pitting, which is caused principally by the electrochemical potential differences of different phases [4]. As the main strengthening phase, the Mg-Si phase has a complicated potential compared to Al. When the concentration of NaCl is lower, it becomes the anode in the system and is corroded before the matrix. It dissolves into the electrolyte selectively [5]. When the concentration of NaCl increases, the Mg-Si phase becomes the cathode in the system. The reason is that at the beginning of corrosion Mg ions are more active and migrate more rapidly into the electrolyte. The Mg-Si phase decomposes and this causes the enrichment of Si. As Si has a more positive potential than Al, the Mg-Si phase becomes the cathode. In addition, previous studies indicate that the ageing treatment has a significant impact on the corrosion resistance of Al alloys, including $2 \times \times \times$ series Al alloys [6], $6 \times \times \times$ series Al alloys [7], and $7 \times \times \times$ series Al alloys [8].

It is observed that the addition of Cu has a negative effect on the corrosion resistance of Al alloy. Al alloys of high Cu content (>2 wt%) are reported to aggravate localized corrosion, such as pitting corrosion [9,10] and exfoliation corrosion [11,12] on the alloy surface. With the growing of pitting phenomena, it could encourage the intergranular corrosion, which spreads rapidly in the interior of the alloy. The process of dealloying of Cu-enriched intermetallic precipitation is detected in Al alloy within a chloride solution, which facilitates the corrosion propagation process [13]. The corrosion process is influenced by the distribution of Cu in the microstructure. The initiation of pitting corrosion usually occurs near the Cu-enriched precipitates on the surface of the Al matrix [14] because these particles have a potential difference with the matrix. The galvanic reaction between them accelerates the localized pitting corrosion.

This study aims to investigate the effect of Cu addition on an Al-Si-Mg cast alloy. The corrosion behavior of the alloys under different ageing stages is investigated. Corrosion experiments are carried out by both the full immersion test and electrochemical measurements at ambient temperature. Scanning electron microscope (SEM) and transmission electron microscope (TEM) are applied to characterize the surface microstructure before and after corrosion to acquire a better knowledge of the corrosion mechanism.

2. Experimental Section

Two kinds of cast alloys are investigated for this study, whose chemical components are shown in Table 1 below. The alloys are obtained through a die casting process. The alloys are cut into the samples of 10 mm × 10 mm × 2 mm by the wire-electrode cutting machine. Samples are heated to 540 °C, held for 8 h, followed by water quenching and artificial ageing at 175 °C for different durations from 0 to 30 h. The hardness at different ageing times is measured by a Vickers indenter with a force of 5 kg and the dwell time of 15 s. For each Sample, 5 test points were taken on the flat surface to calculate the average value as the final hardness and draw the ageing curve. Sample surfaces are observed by SEM and TEM before corrosion. Samples subjected to SEM observation are prepared by grinding with silicon carbide abrasive papers with grit sizes of 240, 400, 800, and 1000, followed by cloth polishing using 3 and 1 µm diamond suspension solutions. They are then etched by HF solution for several seconds. Samples for TEM were ground and electropolished using a twin-jet electropolisher operated at 20 V and 60–100 mA at the temperature below −25 °C in a solution of 30 vol.% HNO₃ and 70 vol.% methanol. Atomic-resolution high-angle annular dark-field scanning transmission electron microscope (HAADF-STEM) imaging and energy dispersive X-Ray spectroscopy (EDS) mapping was carried out on JEM-ARM200F (JEMARM200F, JEOL Ltd., Tokyo, Japan), equipped with a probe-Cs corrector and a cold field emission gun. The accelerating voltage was 200 kV. The HAADF-STEM images are acquired with a collection semi-angle of 68–280 mrad.

Table 1. Chemical composition of Al alloy specimens (wt.%).

Element	Si	Mg	Cr	Cu	Fe	Al
Al-Si-Mg-Cr	7	0.3	0.3	0	<0.15	Bal.
Al-Si-Mg-Cr-Cu	7	0.3	0.3	1.5	<0.15	Bal.

An electrochemical workstation is used to measure the sample open circuit potential and polarization voltage in 3.5 wt.% NaCl solution. All the electrochemical measurements are used with a three-electrode electrochemical cell, with sample as the working electrode (WE), a saturated calomel electrode (SCE) as the reference electrode (RE), and a platinum electrode as the counter electrode (CE). Weight loss is calculated after 10 days, 20 days, and 30 days of immersion in 3.5 wt.% NaCl solution. The microstructures are observed by SEM after 30 days immersion.

3. Results and Discussion

3.1. Hardness

Hardness curves of different samples are studied to relate the corrosion resistance with the ageing time, which affects the amount and the distribution of the precipitation phase. Figure 1 is the ageing curves of two alloys. The addition of Cu notably improves the hardness of quenched samples from 55 Hv to 71 Hv and also the peak hardness from 105 Hv to 115 Hv [15]. The ageing time for the sample with Cu where the hardness attains the peak is around 3 h longer than that of the alloy without Cu. For each sample, underaged, peak-aged, and overaged samples are chosen to be studied.

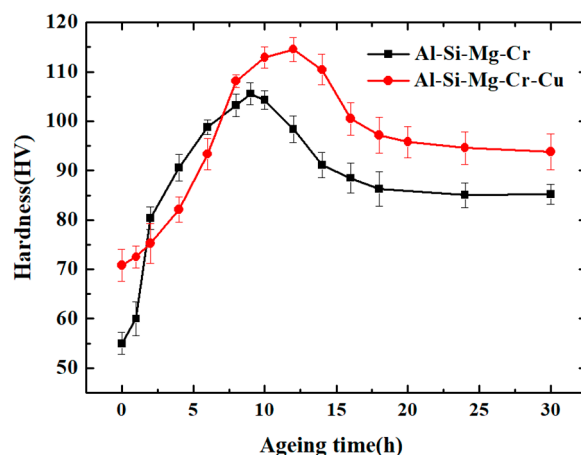


Figure 1. Ageing curves of Al-7%Si-0.3%Mg-0.3%Cr alloy and Al-7%Si-0.3%Mg-0.3%Cr-1.5%Cu alloys.

3.2. Open Circuit Potential

In Figure 2a, the results of the open circuit potential (OCP) measurements show that overaged and underaged samples are less likely to be corroded than that one of peak age. It is ranked as follows: 12 h \approx 1 h > 9 h > 2 h > 6 h. However, the range of OCP is about $-0.76 \sim -0.74$ V, which means the effect of ageing time on corrosion resistance is not significant. But in Figure 2b, the OCP is ranked as follows: 1 h > 6 h > 2 h > 16 h > 12 h, the range $-0.84 \sim -0.62$ V is much larger, which means the ageing time is more important for the corrosion resistance Al-7%Si-0.3%Mg-0.3%Cr-1.5%Cu alloy. As the ageing time affect most importantly the precipitation in the matrix, therefore the particles containing Cu affect the corrosion resistance. For peak-ageing samples (9 h in (a) and 12 h in (b)), the OCP in (a) is -0.74 V and in (b) is -0.84 V, which is to say that the addition of Cu increases the tendency to be corrode for Al alloys.

Figure 2c shows the polarization kinetics curve of the Al-7%Si-0.3%Mg-0.3%Cr alloy in a 3.5% NaCl solution. In general, the anode polarization branch represents the anode dissolution in the solution, and the cathodic polarization branch represents the cathodic hydrogen evolution via the water. The trend of different curves in the figure are consistent, and the corrosion potentials of all samples are distributed between -1.2 and -1.0 V. There is no obvious passivation phenomenon formation and passivation film breakdown process on the anode branch of the curve. The polarization corrosion potential is as follows: 12 h > 1 h > 9 h > 2 h > 6 h. The relative relationship of the potential is basically consistent with the measurement of the open circuit potential. Figure 2d shows the polarization kinetics curve of the Al-7%Si-0.3%Mg-0.3%Cr-1.5%Cu alloys in a 3.5% NaCl solution. The corrosion potentials of samples are distributed between -0.6 V and -0.75 V, and the values are close to the open circuit potential. Except for the sample aged for one hour, the corrosion potentials of other samples are very close. The corrosion potential of the sample under ageing treatment for 1 h is significantly higher than that of others, indicating a weak trend of corrosion. The trend of the anode branch of all curves is similar to that of the curves without adding Cu, and there is no obvious passivation and breakdown process.

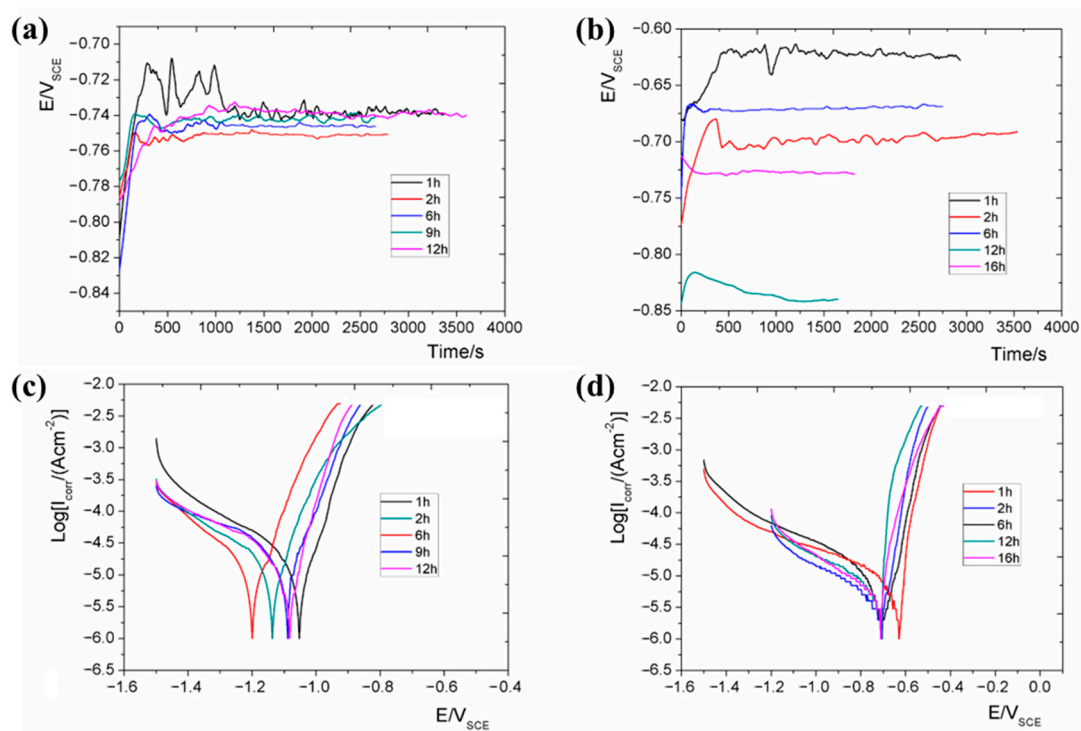


Figure 2. Open circuit potentials of (a) Al-7%Si-0.3%Mg-0.3%Cr alloy and (b) Al-7%Si-0.3%Mg-0.3%Cr-1.5%Cu alloy and Tafel plots of (c) Al-7%Si-0.3%Mg-0.3%Cr alloy and (d) Al-7%Si-0.3%Mg-0.3%Cr-1.5%Cu alloy in a 3.5% NaCl solution after different ageing time.

According to the chosen Tafel sections of polarization curves, it was very convenient to calculate the corresponding corrosion current density (I_{corr}), polarization resistance (R_p) and corrosion rate (CR). The corrosion current density, I_{corr} ($\mu\text{A}\cdot\text{cm}^{-2}$) could be estimated by Tafel extrapolation method [16]. The corrosion rate (CR_i , $\text{mm}\cdot\text{y}^{-1}$) could be calculated by the I_{corr} according to ASTM G102-89 (2015) [17]:

$$CR_i = K_i \frac{I_{corr}}{\rho} EW \quad (1)$$

where, CR_i is the corrosion rate calculated by polarization curve, K_i is a constant ($3.27 \times 10^{-3} \text{ mm}\cdot\text{g}\cdot\mu\text{A}^{-1}\cdot\text{cm}\cdot\text{y}$), ρ is the material density, I_{corr} is the corrosion current density, and EW is the equivalent weight.

According to ASTM G102-89 (2015), the polarization resistance (R_p , $\text{k}\Omega$) could be calculated by the following equation:

$$R_p = \frac{\beta_a \beta_c}{2.3(\beta_a + \beta_c) I_{corr}} \quad (2)$$

where, β_a and β_c are the slopes of Tafel regions of the logarithmic anodic and cathodic polarization curves respectively, I_{corr} is the corrosion current density.

The calculated values of polarization curves are presented in Table 2. Table 2 shows the corrosion potential and corrosion current density of Al-7%Si-0.3%Mg-0.3%Cr alloy and Al-7%Si-0.3%Mg-0.3%Cr-1.5%Cu alloy with different ageing time. It can be seen from Table 2 that the corrosion potentials (E_{corr}) of alloys have a similar variation trend. The E_{corr} became more negative with the increasing ageing time of the samples. Then E_{corr} changes towards a positive direction with further increase in the ageing time. The maximum corrosion potential of Al-7%Si-0.3%Mg-0.3%Cr alloys appears before peak-ageing (6 h), while the maximum corrosion potential of Al-7%Si-0.3%Mg-0.3%Cr-1.5%Cu alloys appears at peak-ageing (12 h). Similarly, the corrosion current density (I_{corr}) also presents the same

characteristics. Before peak-ageing, the I_{corr} increases significantly with the increasing ageing time of the sample, indicating that increased ageing time could effectively increase the corrosion rate. After peak-ageing, the I_{corr} decreases with the increasing ageing time of the sample. The difference in E_{corr} and I_{corr} between the two alloys may be due to the addition of Cu. It will be further discussed below.

Table 2. Tafel polarization data for Al-7%Si-0.3%Mg-0.3%Cr alloy and Al-7%Si-0.3%Mg-0.3%Cr-1.5%Cu alloy.

Samples	Ageing Time (h)	E_{corr} (mVSCE)	I_{corr} ($\mu\text{A}/\text{cm}^2$)	R_p ($\text{k}\Omega$)	CR ($\text{mm}\cdot\text{y}^{-1}$)
Al-7%Si-0.3%Mg-0.3%Cr	1 h	−1.0824	4.1637	4.3231	0.04533
	2 h	−1.1374	5.4485	3.3037	0.05932
	6 h	−1.2002	8.7132	2.0658	0.09487
	9 h	−1.0892	4.1056	4.3843	0.04470
	12 h	−1.0527	3.6887	4.8798	0.04016
Al-7%Si-0.3%Mg-0.3%Cr-1.5%Cu	1 h	−0.6306	9.6664	1.8621	0.10525
	2 h	−0.7024	10.5875	1.7001	0.11528
	6 h	−0.7048	11.0477	1.6293	0.12029
	12 h	−0.7103	14.0117	1.2846	0.15256
	16 h	−0.7064	13.6173	1.3218	0.14827

According to the corrosion current density and corresponding electrochemical corrosion rate calculated by the Tafel extrapolation method, the Al-7%Si-0.3%Mg-0.3%Cr alloy aged for 6 h has the highest corrosion rate, with the corrosion rate is ranked as follows: 6 h > 2 h > 1 h > 9 h > 12 h. According to the corrosion current density and corresponding electrochemical corrosion rate calculated by the Tafel extrapolation method, the Al-7%Si-0.3%Mg-0.3%Cr-1.5%Cu alloy with peak ageing of 12 h has the highest corrosion rate, with the corrosion rate is ranked as follows: 12 h > 16 h > 6 h > 2 h > 1 h. This indicates that under the action of an applied electric field, peak-aged alloys exhibit the fastest corrosion rate, followed by over-aged alloys, and under-aged alloys exhibit a slower corrosion rate. This result is consistent with the measurement of open circuit potential. Compared with the sample without Cu addition, the corrosion rate is significantly accelerated.

3.3. Immersion Weight Loss

According to the immersion weight loss after 10 days, 20 days, and 30 days in NaCl solution, corrosion rates are calculated and shown in Figure 3. For both alloys, the corrosion rates slow down as the immersion time extends. And samples with peak-ageing time have the greatest corrosion rate. On comparing the two kinds of alloys, the addition of Cu increased the corrosion rate by 2~3 times for samples with different ageing conditions.

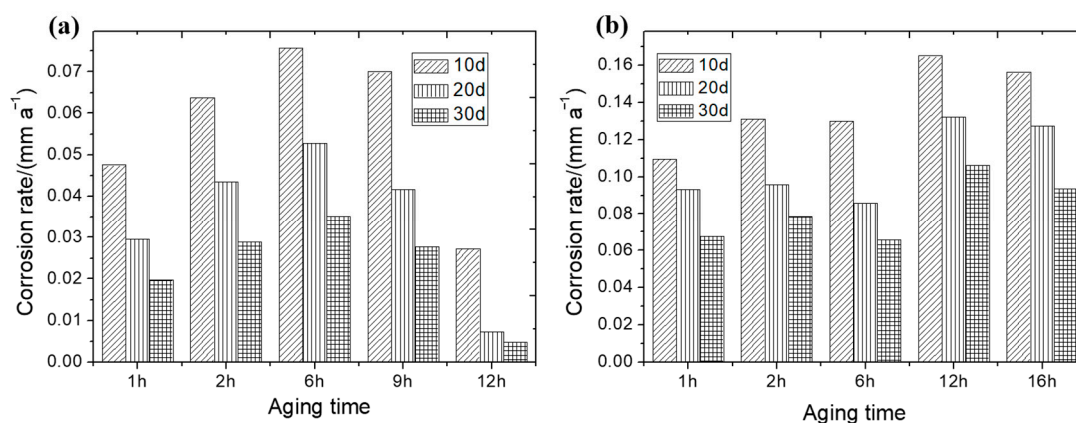


Figure 3. Immersion corrosion rates of (a) Al-7%Si-0.3%Mg-0.3%Cr alloy and (b) Al-7%Si-0.3%Mg-0.3%Cr-1.5%Cu alloy alloys after different ageing time.

3.4. Microstructures before and after Immersion by SEM and EDS

Figures 4 and 5 are SEM images of samples of various ageing time. The two kinds of alloys are similar in morphology with Si-enriched second phase near the grain boundary. Some of these Si-enriched phases have been identified as $\text{Al}_{13}\text{Cr}_4\text{Si}_4$ phase in our previous work [2]. The matrix has a dendrite-shaped structure which is more and more obvious as the ageing time extends. No apparent difference in the microstructures can be observed with the addition of Cu before immersion corrosion.

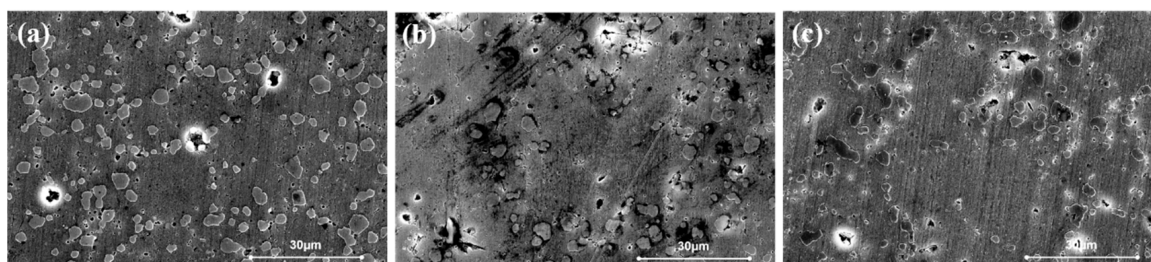


Figure 4. Microstructures of Al-7%Si-0.3%Mg-0.3%Cr alloy aged at 175 °C for (a) 1 h, (b) 6 h, (c) 12 h.

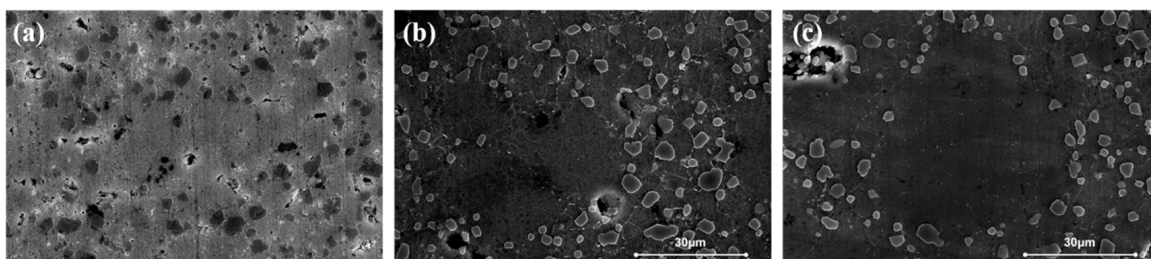


Figure 5. Microstructures of Al-7%Si-0.3%Mg-0.3%Cr-1.5%Cu alloy aged at 175 °C for (a) 1 h, (b) 12 h, (c) 16 h.

Figures 6 and 7 are SEM images of alloys after 30-days immersion corrosion in 3.5 wt.% NaCl solution. Compared with SEM images before corrosion, the difference between the two alloys are much more obvious. In Figure 6, pitting is more uniformly distributed on the matrix than that in Figure 7, especially for underaged and overaged samples (Figure 6a,e). Around the pitting, the structure is likely to peel and exfoliate on the surface. The diameters of the pitting holes of the peak-aged sample (Figure 6c) are greater than those of the others, which indicates that pitting probably begins near the precipitation phase.

Figure 8 shows the microstructure and EDS mapping of Al-7%Si-0.3%Mg-0.3%Cr alloy after 30-days immersion, while Figure 9 shows the microstructure and EDS mapping of Al-7%Si-0.3%Mg-0.3%Cr-1.5%Cu alloy after 30-days immersion. In the higher magnification images for peak-aged and overaged samples (Figure 6d,f), brighter particles are observed on the surface, which is believed to be Si-enriched according to EDS results shown in Figure 8. In Figures 7 and 9, pitting and Si-enriched particles are more obvious. The pitting is deeper and bigger for peak-aged and overaged samples (Figure 7d,f). Intergranular corrosion develops near and inside the pitting holes because of the addition of Cu. Plenty of Si-enriched particles are left due to the dealloying of intermetallic phases. As the pitting corrosion essentially was attributable to Si-enriched particles. The driving force of the localized corrosion at the interface between constituent cathodic particles and the matrix of Al alloys is the galvanic coupling between the particles and the matrix. Segregation of Cu on the surface of the particles was observed, as marked by arrows in Figure 9c. We detected similar phenomena in previous studies that the precipitates $\eta\text{-Mg}(\text{Zn}, \text{Cu})_2$ form on the surface of $\text{Al}_{18}\text{Mg}_3(\text{Cr}, \text{Mn})_2$ dispersoids during ageing treatment [8]. The morphological characteristic of a simple cathodic particles/anodic matrix system after corrosion is a hole attributed to the matrix dissolution around an almost unattacked particle.

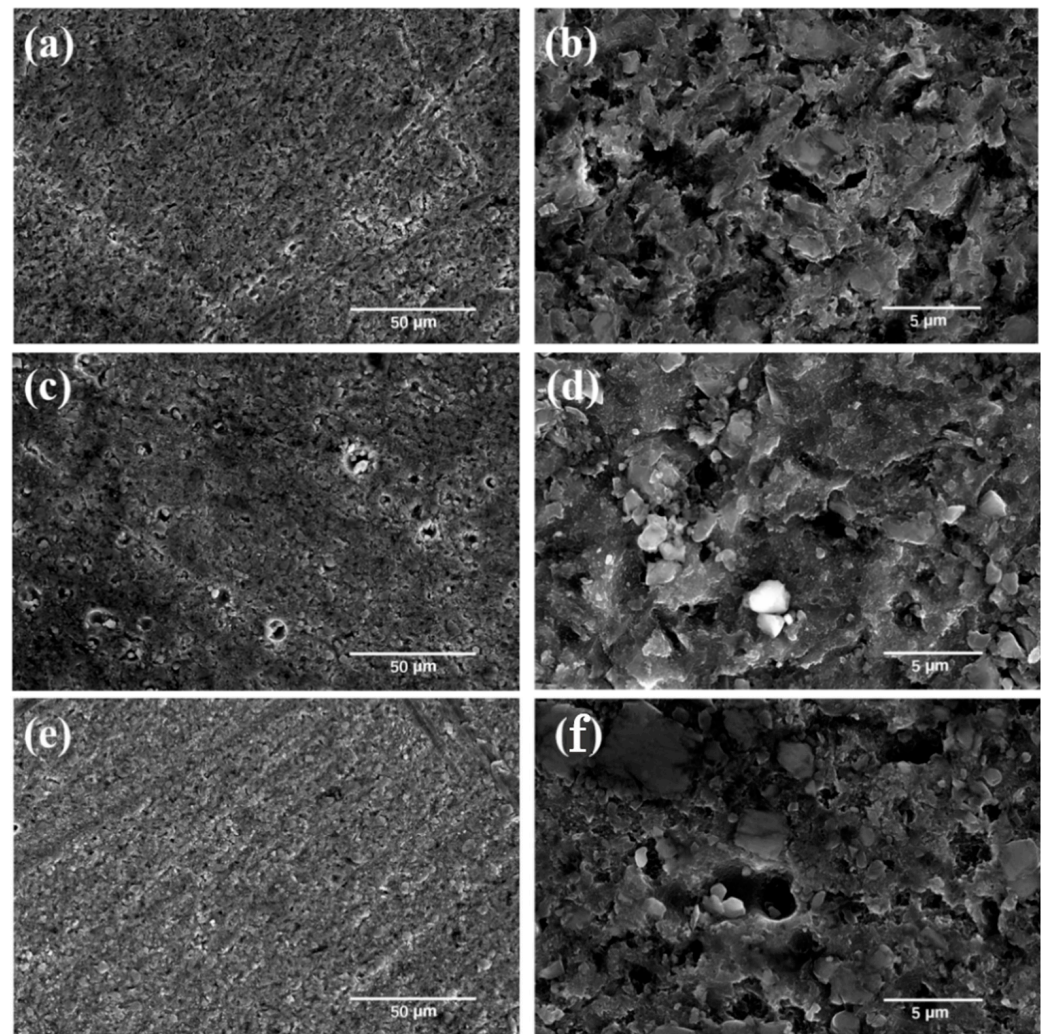


Figure 6. SEM images of the corrosion surfaces of Al-7%Si-0.3%Mg-0.3%Cr alloy aged at 175 °C for (a,b) 1 h, (c,d) 6 h, (e,f) 12 h after immersion for 30-days.

3.5. Microstructural Observation by TEM

Figure 10 shows the TEM images for two alloys with under-ageing, peak-ageing, and over-ageing conditions. In Figure 10a, precipitation of a small diameter, which is the GP zone, is distributed intensively in the matrix of underaged Al-7%Si-0.3%Mg-0.3%Cr alloy. Saturated Si and Mg begin to form the Mg-Si phase and other precipitation, which has a difference in potential and causes electrochemical corrosion. The peak-aged alloy sample (Figure 10b) has fewer particles but plenty of needle-shaped precipitation instead. They grow into stick-shape in overaged conditions (Figure 10c). In Figure 10d,e, the microstructures of Al-7%Si-0.3%Mg-0.3%Cr-1.5%Cu alloy resemble those of Al-7%Si-0.3%Mg-0.3%Cr alloy. However the overaged microstructure has thicker needle-shaped precipitation. Previous studies show that it contains Si, Mg, and Cu [15]. And another plate-shaped precipitation phase θ'' (GP II zones)- Al_3Cu or θ' - Al_2Cu also appears during ageing [15]. The phase has a more positive potential than the Al matrix in NaCl solution, thus the matrix near this phase tends to be corroded and pit.

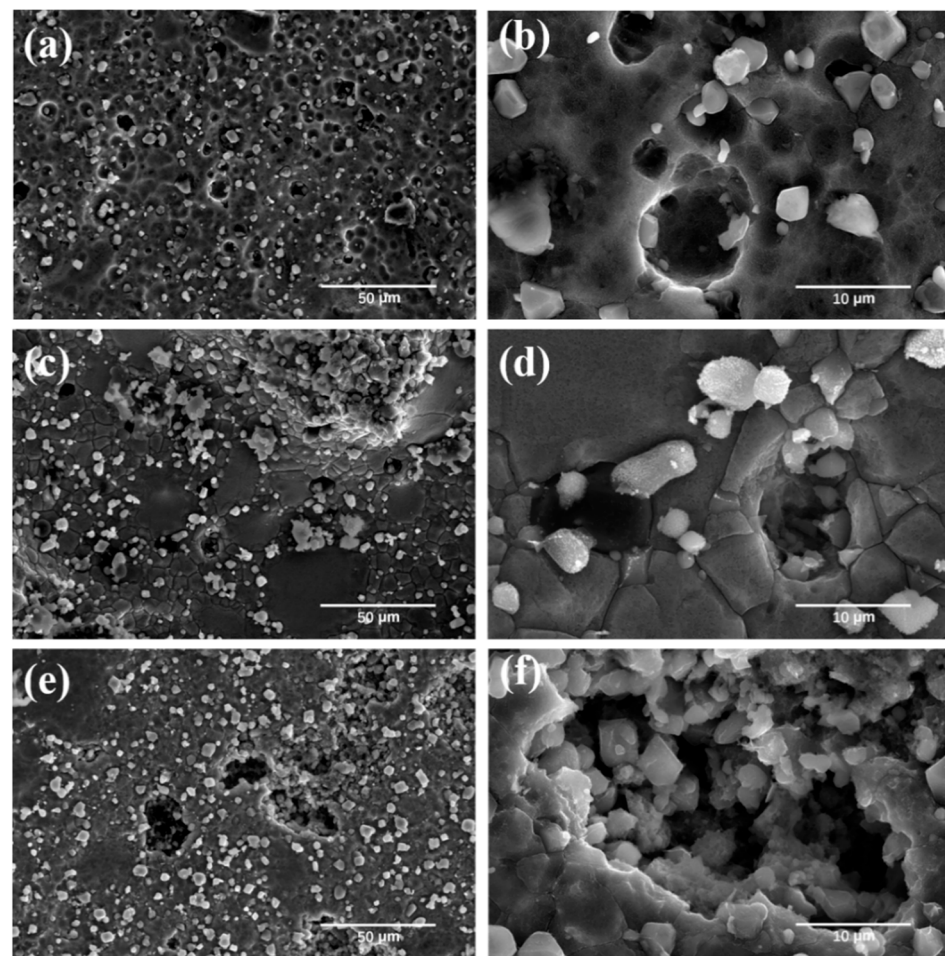


Figure 7. SEM images of the corrosion surfaces of Al-7%Si-0.3%Mg-0.3%Cr-1.5%Cu alloy aged at 175 °C for (a,b) 1 h, (c,d) 6 h, (e,f) 12 h after immersion for 30-days.

The HAADF-STEM imaging combined with EDS analysis was performed in order to further identify the precipitates. Figure 11a shows the typical low-magnification HAADF-STEM image, it is apparent that the alloy contains dispersive dot-like and needle-like precipitates. It is well known that the intensity in HAADF-STEM images is approximately proportional to $Z^{1.7}$, and Z is the atomic number. There is no doubt that these precipitates contain at least one element heavier than Al because its contrast is much brighter. Figure 11d–f shows the EDS spectrums from the Al matrix, dot-like and needle-like precipitates, respectively, inserts are the corresponding contents of elements. The EDS results from dot-like precipitates show that the atomic percent concentration of the Mg, Si, and Cu is much higher than that of the matrix. It was determined that the content of Cu in needle-like precipitates is the highest of all, but its contents of Mg and Si are very low. In regard to HAADF-STEM images and EDS results, the dot-like precipitates are estimated to be β'' -Mg₅Si₆ precipitates while the needle-like precipitates are estimated to be θ'' (GP II zones)-Al₃Cu precipitates. The atomic-scale HAADF-STEM is applied to further characterize the precipitates. Figure 11b,c shows the enlarged HAADF-STEM images of dot-like and needle-like precipitates from the Figure 11a, respectively. By observing the precipitates from the directions of $[001]_{Al}$, as shown in Figure 11b,c and matching to the atomic models, it can be confirmed that these precipitates are β'' and θ'' , respectively. As shown in Figure 10b, this precipitate has a monoclinic lattice, $a = 1.51$ nm, $b = 0.405$ nm, $c = 0.67$ nm, $\beta = 105^\circ$, which is identified as that of β'' in Cu-free alloys [18,19]. It was determined that Cu atoms diffuse into β'' and occupy in a specific position of β'' unit cell, as shown by dotted red circle in Figure 11b. Some of Si and Mg, Al in β'' lattice are replaced by Cu atoms. There

are atomic columns inside precipitate present high contrast, as enclosed by red ellipses. It shows that Cu occupies Si3/Al site of β'' . Meanwhile, many Cu atoms are observed to segregate at the edge of β'' . This is consistent with the EDS results that Cu is determined to be enriched in the β'' .

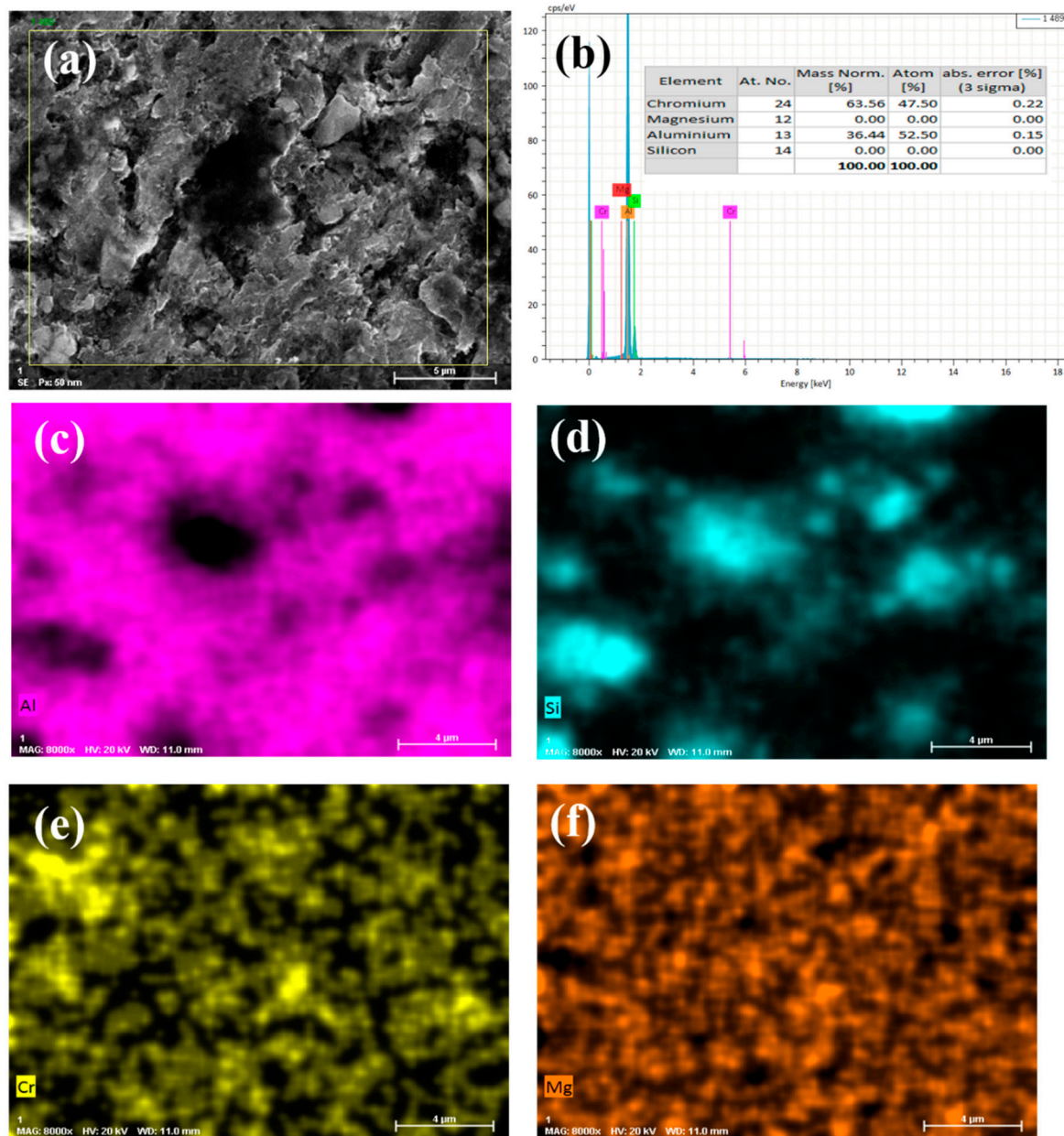


Figure 8. Microstructure and EDS mapping of Al-7%Si-0.3%Mg-0.3%Cr alloy after 30-days immersion, (a) 8000 \times , (b) EDS results, and corresponding EDS maps of elements (c) Al, (d) Si, (e) Cr, (f) Mg.

As discussed above, the correlation between Cu and corrosion properties can be obtained as follows. With the formation of precipitates, there are electrochemical potentials between the precipitates and the Al matrix. This leads to the gradual decrease of the corrosion resistance of the alloy with increasing ageing time. It is well known that the Cu-rich phases such as θ'' phase act as a cathode that can accelerate the localized corrosion of Al alloys by promoting fast anodic dissolution of the surrounding Al matrix, resulting in the deterioration of corrosion resistance of the alloy. In addition, Cu atoms both replaced some of Si and Mg, Al in (Si3/Al site of) β'' precipitates and segregates in the edge of β'' precipitates, resulting in an increase of electrochemical potentials between the β''

precipitates and the Al matrix. In addition, according to our previous work [20], a Cu-enriched layer forms in the corroded surface of the sample as the corrosion goes on. It is believed that the deterioration of corrosion performance partly is attributed to the Cu-enriched precipitates as a result of galvanic coupling between the precipitates and the matrix.

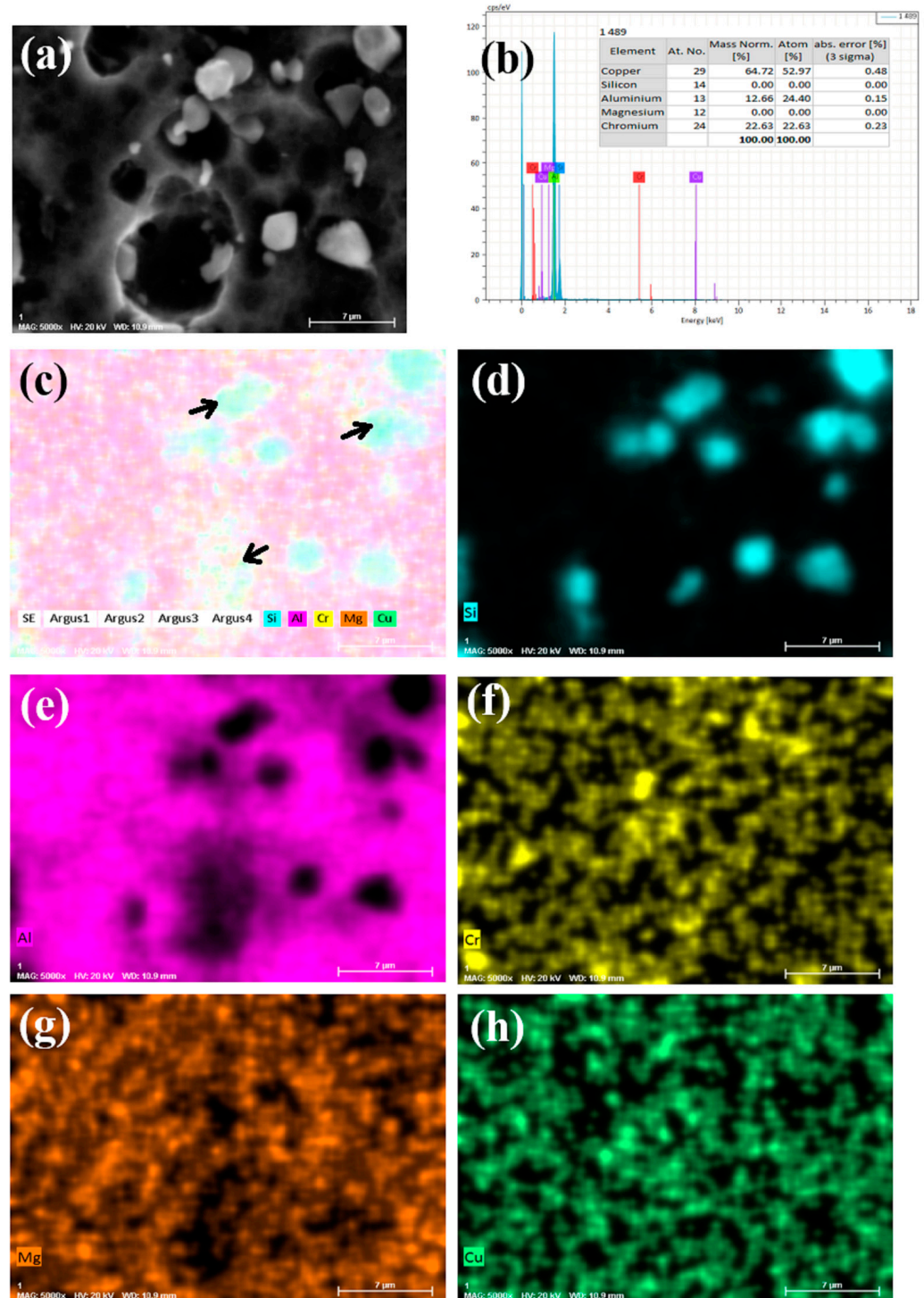


Figure 9. Microstructure and EDS mapping of Al-7%Si-0.3%Mg-0.3%Cr-1.5%Cu alloy after 30-days immersion, (a) 5000 \times , (b) EDS results, and corresponding EDS maps of elements (c) all elements, (d) Si, (e) Al, (f) Cr, (g) Mg, (h) Cu.

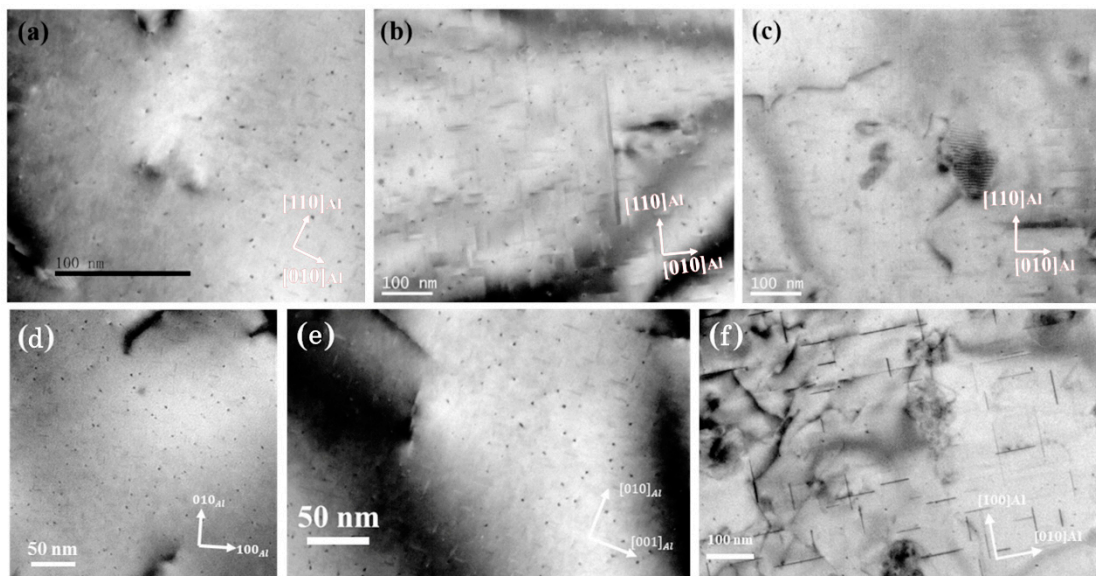


Figure 10. Microstructures of Al-7%Si-0.3%Mg-0.3%Cr alloy with 175 °C ageing by (a) 1 h, (b) 6 h, (c) 12 h and Al-7%Si-0.3%Mg-0.3%Cr-1.5%Cu alloy with 175 °C ageing by (d) 1 h, (e) 12 h, (f) 16 h.

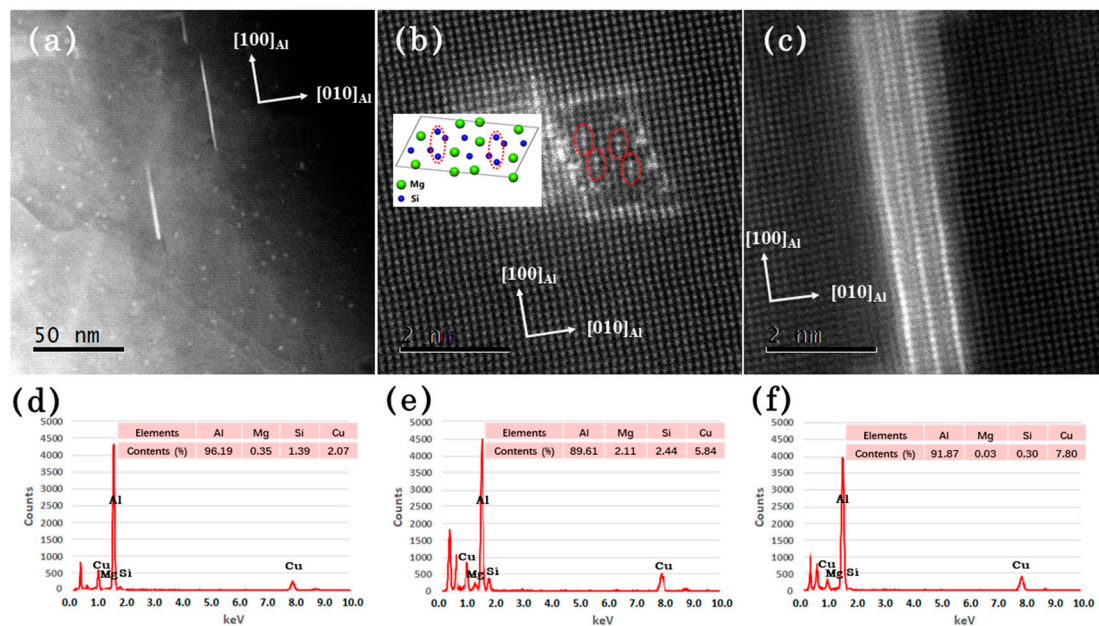


Figure 11. Low magnification HAADF-STEM images of Al-7%Si-0.3%Mg-0.3%Cr-1.5%Cu alloy (a), atomic resolution HAADF-STEM images of β'' (b) and θ'' (c), and EDS spectrums of Al matrix (d), β'' (e) and θ'' (f).

As discussed above, the deterioration of corrosion performance of alloy with the addition of Cu is essentially attributed to the Si-enriched $\text{Al}_{13}\text{Cr}_4\text{Si}_4$ particles with segregation of Cu on its surface and the Cu-enriched precipitates, β'' - Mg_5Si_6 precipitates and θ'' - Al_3Cu precipitates.

4. Conclusions

In this work, Al-7%Si-0.3%Mg-0.3%Cr alloy and Al-7%Si-0.3%Mg-0.3%Cr-1.5%Cu alloy are studied to understand the effect of Cu addition on corrosion resistance. Hardness curves are traced first to determine suitable parameters for heat treatment. Corrosion experiments are carried out by electrochemical workstation and by immersion method in

3.5 wt.% NaCl solution. SEM and TEM images are taken before and after the immersion experiment to identify the surface microstructures. The conclusions are as follows:

(1) The corrosion resistance of alloy samples during artificial ageing varies with the ageing time. The two alloys selected in this study have the worst corrosion resistance at peak ageing time. The main reason is that there is a potential difference between the precipitated phase and the alloy matrix. At the peak ageing time, the number of precipitated phases is the largest and most evenly distributed, forming a galvanic pair, thereby speeding up the corrosion rate.

(2) The addition of Cu can increase the peak hardness of the Al-7%Si-0.3%Mg-0.3%Cr alloy by 9.5%. However, the addition of Cu reduces significantly the corrosion resistance of the alloy. The addition of Cu accelerates the immersion corrosion rate for 30 days by 201.5% for the peak ageing samples. The effect of the 12 h peak ageing sample and 16 h over-aging sample is more significant.

(3) β'' -Mg₅Si₆ precipitates and θ'' -Al₃Cu precipitates are observed by HAADF-STEM in Al-7%Si-0.3%Mg-0.3%Cr-1.5%Cu alloy. The Cu atoms occupy Si₃/Al site of β'' segregates at the edge of β'' . It is believed that the deterioration of corrosion performance essentially is attributed to the Si-enriched Al₁₃Cr₄Si₄ particles with segregation of Cu on its surface and the Cu-enriched precipitates, β'' -Mg₅Si₆ precipitates and θ'' -Al₃Cu precipitates.

Author Contributions: Conceptualization, B.C. and B.H.; investigation, Z.W., L.D. and B.C.; writing—original draft preparation, Z.W. and B.C.; writing—review and editing, B.C. All authors have read and agreed to the published version of the manuscript.

Funding: This research received no external funding.

Institutional Review Board Statement: Not applicable.

Informed Consent Statement: Not applicable.

Data Availability Statement: Data is contained within the article.

Conflicts of Interest: The authors declare no conflict of interest.

References

1. Itoh, G.; Suzuki, T.; Horikawa, K. Effects of alloy composition and quenching rate on the bendability in Al-Mg-Si alloys. In *Materials Science Forum*; Trans Tech Publications Ltd.: Zurich, Switzerland, 2002; pp. 1193–1198.
2. Wang, S.; Dong, L.; Han, X.; Fan, Y.; Chen, B. Orientations and interfaces between α' -Al₁₃Cr₄Si₄ and the matrix in Al-Si-Cr-Mg alloy. *Mater. Charact.* **2020**, *160*, 110096. [\[CrossRef\]](#)
3. Marioara, C.; Andersen, S.; Stene, T.; Hasting, H.; Walmsley, J.; Van Helvoort, A.; Holmestad, R. The effect of Cu on precipitation in Al-Mg-Si alloys. *Philos. Mag.* **2007**, *87*, 3385–3413. [\[CrossRef\]](#)
4. Grilli, R.; Baker, M.A.; Castle, J.E.; Dunn, B.; Watts, J.F. Localized corrosion of a 2219 aluminium alloy exposed to a 3.5% NaCl solution. *Corros. Sci.* **2010**, *52*, 2855–2866. [\[CrossRef\]](#)
5. Eckermann, F.; Suter, T.; Uggowitzer, P.J.; Afseth, A.; Schmutz, P. The influence of MgSi particle reactivity and dissolution processes on corrosion in Al-Mg-Si alloys. *Electrochim. Acta* **2008**, *54*, 844–855. [\[CrossRef\]](#)
6. Zou, Y.; Chen, X.; Chen, B. Corrosion behavior of 2198 Al-Cu-Li alloy in different aging stages in 3.5 wt% NaCl aqueous solution. *J. Mater. Res.* **2018**, *33*, 1011–1022. [\[CrossRef\]](#)
7. Li, W.; Chen, X.; Chen, B. Effect of aging on the corrosion behavior of 6005 Al alloys in 3.5 wt% NaCl aqueous solution. *J. Mater. Res.* **2018**, *33*, 1830–1838. [\[CrossRef\]](#)
8. Fang, L.; Zheng, J.-x.; Xia, C.; Xu, X.-s.; Bin, C. Study on corrosion resistance of artificially aged 7075 aluminium alloy by using Cs-corrected STEM. *Trans. Nonferrous Met. Soc. China* **2022**, *32*, 2828–2837.
9. Wang, S.-S.; Huang, I.-W.; Yang, L.; Jiang, J.-T.; Chen, J.-F.; Dai, S.-L.; Seidman, D.N.; Frankel, G.; Zhen, L. Effect of Cu content and aging conditions on pitting corrosion damage of 7xxx series aluminum alloys. *J. Electrochem. Soc.* **2015**, *162*, C150–C160. [\[CrossRef\]](#)
10. Marlaud, T.; Malki, B.; Henon, C.; Deschamps, A.; Baroux, B. Relationship between alloy composition, microstructure and exfoliation corrosion in Al-Zn-Mg-Cu alloys. *Corros. Sci.* **2011**, *53*, 3139–3149. [\[CrossRef\]](#)
11. Zhao, X.; Frankel, G.S. Quantitative study of exfoliation corrosion: Exfoliation of slices in humidity technique. *Corros. Sci.* **2007**, *49*, 920–938. [\[CrossRef\]](#)
12. Meng, Q.; Frankel, G. Effect of Cu content on corrosion behavior of 7xxx series aluminum alloys. *J. Electrochem. Soc.* **2004**, *151*, B271–B283. [\[CrossRef\]](#)

13. Buchheit, R.; Martinez, M.; Montes, L. Evidence for Cu Ion Formation by Dissolution and Dealloying the Al₂CuMg Intermetallic Compound in Rotating Ring-Disk Collection Experiments. *J. Electrochem. Soc.* **2000**, *147*, 119–124. [[CrossRef](#)]
14. Lunarska, E.; Trela, E.; Szklarska-Smialowska, Z. Pitting corrosion of powder metallurgy AlZnMg alloys. *Corrosion* **1987**, *43*, 219–228. [[CrossRef](#)]
15. Chen, B.; Dong, L.; Hu, B.; Liu, Z. The Effect of Cu Addition on the Precipitation Sequence in the Al-Si-Mg-Cr Alloy. *Materials* **2022**, *15*, 8221. [[CrossRef](#)] [[PubMed](#)]
16. Shi, Z.; Liu, M.; Atrens, A. Measurement of the corrosion rate of magnesium alloys using Tafel extrapolation. *Corros. Sci.* **2010**, *52*, 579–588. [[CrossRef](#)]
17. ASTM Standard G102-89; Standard Practice for Calculation of Corrosion Rates and Related Information from Electrochemical Measurements. ASTM International: West Conshohocken, PA, USA, 2015.
18. Zandbergen, H.W. Structure Determination of Mg₅Si₆ Particles in Al by Dynamic Electron Diffraction Studies. *Science* **1997**, *277*, 1221–1225. [[CrossRef](#)]
19. Andersen, S.J.; Zandbergen, H.W.; Jansen, J.; Traeholt, C.; Tundal, U.; Reiso, O. The crystal structure of the β'' phase in Al-Mg-Si alloys. *Acta Mater.* **1998**, *46*, 3283–3298. [[CrossRef](#)]
20. Wang, Z.; Lv, K.; Zheng, J.K.; Chen, B. Atomic-scale characterization of interfaces between 2A70 aluminum alloy matrix and Cu-enriched layer after electropolishing. *Mater. Charact.* **2019**, *150*, 150–154. [[CrossRef](#)]

Disclaimer/Publisher's Note: The statements, opinions and data contained in all publications are solely those of the individual author(s) and contributor(s) and not of MDPI and/or the editor(s). MDPI and/or the editor(s) disclaim responsibility for any injury to people or property resulting from any ideas, methods, instructions or products referred to in the content.